

VOS-GAN: Adversarial Learning of Visual-Temporal Dynamics for Unsupervised Dense Prediction in Videos

C. Spampinato^{*,§}, S. Palazzo^{*}, P. D'Oro^{*}, F. Murabito^{*}, D. Giordano^{*}, M. Shah[§]

^{*} Pattern Recognition and Computer Vision (PeRCeive) Lab
University of Catania, Italy
www.perceivelab.com

[§] Center for Research in Computer Vision
University of Central Florida, USA
<http://crcv.ucf.edu>

Abstract. Recent GAN-based video generation approaches model videos as the combination of a time-independent scene component and a time-varying motion component, thus factorizing the generation problem into generating background and foreground separately. One of the main limitations of current approaches is that both factors are learned by mapping one source latent space to videos, which complicates the generation task as a single data point must be informative of both background and foreground content. In this paper we propose a GAN framework for video generation that, instead, employs two latent spaces in order to structure the generative process in a more natural way: 1) a latent space to generate the static visual content of a scene (background), which remains the same for the whole video, and 2) a latent space where motion is encoded as a trajectory between sampled points and whose dynamics are modeled through an RNN encoder (jointly trained with the generator and the discriminator) and then mapped by the generator to visual objects' motion. Additionally, we extend current video discrimination approaches by incorporating in the learning procedure motion estimation and, leveraging the peculiarity of the generation process, unsupervised pixel-wise dense predictions. Extensive performance evaluation showed that our approach is able to a) synthesize more realistic videos than state-of-the-art methods, b) learn effectively both local and global video dynamics, as demonstrated by the results achieved on a video action recognition task over the UCF-101 dataset, and c) accurately perform unsupervised video object segmentation on standard video benchmarks, such as DAVIS, SegTrack and F4K-Fish.

1 Introduction

Generative Adversarial Networks (GANs) [1] are a recent trend in computer vision and machine learning that advanced the state of the art on image and video generation to unprecedented levels of accuracy and realism. New adversarial models [2,3,4,5,6,7,8] are proposed at an accelerating pace, both to increase the diversity and resolution of generated images and to tackle theoretical issues on training and convergence. Additionally, GANs have proved useful in training (or supporting the training of) models from unlabeled data, rising as one of the most promising paradigms for unsupervised learning. GANs have been applied mainly to image generation, which naturally drives

models to learn significant visual features that can be employed in a variety of tasks, such as image classification, object detection and semantic segmentation. This has also opened new frontiers in disentangling video dynamics by leveraging the endless amount of (unlabeled) data available on the web. However, naively extending image generation methods to videos may be too simplistic, as it jointly attempts at handling both the spatial component of the video, describing object and background appearance, and the temporal one, representing object motion and consistency across frames. Building on these considerations, recent generative efforts [9,10] have attempted to factor the latent representation of each video frame into two components that model a time-independent background of the scene and the time-varying foreground elements. We argue that the main limitation of these methods is that both factors are learned by mapping a single point of a source latent space (sampled as random noise) to a whole video. This, indeed, over-complicates the generation task as two videos depicting the same scene with different object trajectories or the same trajectory on different scenes are represented as different points in the latent space, although they share a common factor (in the former case the background, in the latter case object motion). To address this limitation, in this paper we propose a GAN-based generation approach that employs two latent spaces (as shown in Fig. 1) to improve the video generation process: 1) one latent space to model the static visual content of the scene (background), and 2) a foreground latent space to learn object motion dynamics. In particular, these dynamics are modeled as point trajectories in the second latent space, with each point representing the foreground content in a scene and each latent trajectory ensuring regularity and realism of the generated motion across frames. Variations in the scene latent space result in different scenes, while variations in the trajectories of the foreground latent space result in different object motion.

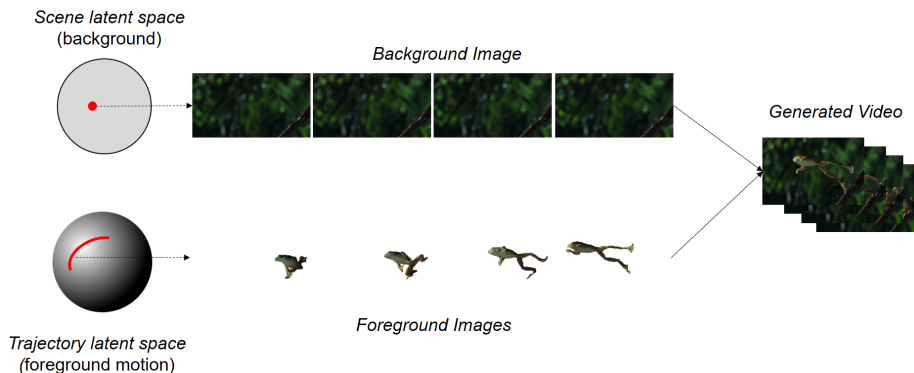


Fig. 1: **Video Generation in VOS-GAN**: we employ a scene latent space to generate background and a foreground latent space to generate object appearance and motion.

The proposed video generation framework consists of a generator/discriminator architecture that creates fixed-length videos by mapping a) a random vector to a static

image (the background) for the whole video, b) a latent-space trajectory (interpolated from two random vectors) representing temporally-consistent motion dynamics, processed by an RNN encoder and then mapped by the generator to visual objects on the background scene. Furthermore, we extend the traditional discriminator architecture in order to perform adversarial dense pixel-wise prediction in videos in an unsupervised way. In particular, besides the adversarial loss driving the generator/discriminator game, we add loss terms related to the estimation of optical flow and segmentation masks by the discriminator from the generated videos. The three losses encourage the generator to produce videos that are indistinguishable from the real ones, while improving learned representations in the discriminator and unlocking the possibility to perform dense video predictions with no (or minimal) additional supervised training.

We demonstrate the effectiveness of the proposed approach by extensively evaluating the realism of the generated videos and the discriminator’s capability to disentangle and learn, in an unsupervised manner, motion dynamics for video action recognition and object segmentation tasks.

Summarizing, the main contributions of this paper are:

- We introduce a GAN-based video generation framework able to explicitly model object motion, with higher quality and realism;
- We verify that our approach is able to learn successfully video features that can be used in a variety of computer vision tasks;
- We demonstrate that our framework provides a useful means for unsupervised dense prediction in videos — known as being an annotation-hungry task — by both employing a trained generator to create synthetic annotated data and directly integrating dense prediction into the adversarial training procedure.

2 Related Work

Until a few years ago, video generation, despite being an intriguing task, was a relatively under-explored topic in computer vision. Recently, thanks to the progress in storage technology and GPUs as well as to the rediscovery of convolutional neural networks, deep generative methods are gaining a lot of attention. Generative adversarial networks (GANs) [1], Variational Autoencoders (VAE) [11] and their combination [12] are among the most investigated solutions, with the former specifically optimized for generative tasks and the latter on learning disentangled representations. In this paper, we focus on GAN-based methods, since VAEs make a strong assumption on the desired output latent distribution. Originally, GANs were proposed for image generation, and since then a large body of adversarial deep generative approaches have been proposed. These models attempt, on one hand, to increase the level of realism [2,3,4] as well as the resolution [2] of the generated images and, on the other hand, to provide solutions to cope with training stabilization issues [5,6,7]. Most of the above methods use a single input latent space to describe all possible visual appearance variations, with some exception, such as Stacked GAN [8] that, instead, employs multiple latent spaces for different image scales. Building on the success of these approaches, [9,10] extended the GAN image generation framework to the video generation problem. In particular, [9] replaced the GAN image generator with a spatio-temporal CNN-based network able to

generate, from an input latent space, background and foreground separately, which are then merged into a video clip for the subsequent discriminator. [10] shares the same philosophy of [9] with the difference that the input latent space is mapped into a set of subspaces, each one used for the generation of a single video frame.

However, simply extending the traditional GAN framework to videos fails since images and videos are intrinsically different because of the time-varying pixels, due to structured object motion, in videos. Despite the above generation methods have exploited video factorization into a stationary and a temporally varying part, deriving the two components from a single input latent space complicates greatly the task, and calls for much more training data given that each point in the input latent space corresponds to a scene with a specific object motion. Furthermore, object motion is only loosely linked to the scene, e.g., the motion of a person walking on two different streets (visual appearance variation) remains more or less the same. Thus, in our opinion, the assumption that the two video components are highly intercorrelated (so as to derive from a single point in the latent space) is too strong, and the approach described in the following Section attempts at disentangling these components.

Recurrent neural networks have been already used for image generation [13], especially to refine results. This differs significantly from our work, where RNNs are used to generate trajectory embeddings that are then transformed to motion-coherent time-varying pixels by a deep neural network consisting of several deconvolution layers. Our RNN-based motion encoder is more similar to those proposed for future frame prediction [14,15,16,17,18,19], which aims at explicitly modeling video dynamics and using the learned embeddings of previous frame to condition the generation process of future frames. The main difference from our work is that they learn dynamics from real data and then draw samples from the learned data distribution; we, instead, learn a latent representation for motion trajectories used for enforcing spatio-temporal consistency.

Beside the generation capabilities, GANs also offer a powerful means for semi-supervised and unsupervised learning. In particular, GANs have been employed for unsupervised domain adaption [20,21], image-to-image translation [22,23] as well as for semi-supervised semantic image segmentation [24]. In the video domain, GANs, instead, have been particularly useful for semi-supervised and unsupervised video action recognition [9,10] or representation learning [25] given their innate ability to learn video dynamics while discriminating between real and fake videos. Indeed, all these methods basically exploit the capability of the discriminator to learn and globally encode video dynamics in a more compact representation, useful for classification. A more complex task, and much less investigated, is, instead, pixelwise dense prediction (e.g., video object segmentation, optical flow estimation, etc.), which requires learning contextual relations between time-varying pixels and large - often unavailable - pixelwise annotated videos. In our work, we employ the proposed video generation framework not only for video action recognition (as most of the existing methods), but also to support pixelwise dense prediction for video object segmentation. While, to the best of our knowledge, ours is the first attempt to perform adversarial video object segmentation (and one of the few CNN-based methods), some GAN-based approaches has been recently proposed to solve the optical flow estimation problem. In particular, [26] proposes a conditional GAN taking an image pair as input and predicting the optical flow.

Flow-warped error images both on predicted flow and on ground-truth flow are then computed and a discriminator is trained to distinguish between the real and the fake ones. The network is trained both on labeled and unlabeled data and the adversarial GAN loss is extended with the supervised end-point-error (EPE) loss, computed on the labeled data. Differently from this work, our dense-prediction network uses only unlabeled data and extends the traditional adversarial loss by including the error made by the discriminator in estimating motion as well as in predicting segmentation maps. In [27], instead, a convolutional neural network is proposed for video object segmentation. Similarly, our segmentation network adopts an encoder-decoder framework by first learning a coarse representation with increasing receptive fields, and then upsampling the learned compact representation using 3D deconvolutional layers, to generate prediction. Beside adversarial training, the main differences between our segmentation network and [27] are: 1) we take videos/images as input, while [27] uses optical flows, thus making its performance too dependent on the upstream optical flow algorithm, and 2) [27] refines results with conditional random field (CRF) [28] pre-trained on pixel-level segmentation task, while we do not perform any supervised post-processing on the prediction maps.

The literature on supervised, semi-supervised and unsupervised video object segmentation (not using CNN-based methods) is wide (see [29] for a comprehensive review) and some of the most recent unsupervised/semi-supervised methods [30,31,32,33,34,35,36] are reported in Sect. 4.4 for comparison.

3 VOS-GAN Model

The video generation architecture presented in this work is based on a GAN framework consisting of the following two modules:

- a *generator*, implemented as a hybrid deep CNN-RNN, that receives two kinds of input: 1) a noise vector from a latent space that models scene background; 2) a sequence of vectors that model foreground motion as a trajectory in another latent space. The output of the generator is a video with its corresponding foreground mask.
- a *discriminator*, implemented as a deep CNN, that receives an input video and 1) predicts whether it is real or not; 2) performs pixel-wise dense prediction to generate an object segmentation map; 3) performs pixel-wise dense prediction to estimate the optical flow between video frames.

The traditional adversarial loss is extended by having the discriminator learn to compute motion-related dense predictions for the input video, thus forcing the generator to produce more realistic motion trajectories. Additionally, this formulation makes the discriminator suitable as a stand-alone model for object segmentation and optical flow estimation.

3.1 Generator Architecture

The architecture of the generator, inspired by the two-stream approach in [9], is shown in Fig. 2. Specifically, our generation approach factorizes the process into separate back-

ground and foreground generation, on the assumption that the world is generally stationary and the presence of informative motion can be constrained only to a set of objects of interest in a semi-static scenery. However, unlike [9], we separate the latent spaces for scene and foreground generation, and explicitly represent the latter as a temporal quantity, thus enforcing a more natural correspondence between the latent input and the frame-by-frame motion output.

Hence, the generator receives two inputs: $z_C \in \mathcal{Z}_C = \mathbb{R}^d$ and $z_M = \{z_{M,i}\}_{i=1}^t$, with each $z_{M,i} \in \mathcal{Z}_M = \mathbb{R}^d$. A point z_C in the latent space \mathcal{Z}_C encodes the general scene to be applied to the output video, and is mainly responsible for driving the *background stream* of the model. This stream consists of a cascade of transposed convolutions, which gradually increase the spatial dimension of the input in order to obtain a full-scale background image $b(z_C)$ that is used for all frames in the generated video.

The set of $z_{M,i}$ points from the latent space \mathcal{Z}_M defines the objects motion to be applied in the video. The latent sequence is obtained by sampling the initial and final points and performing a spherical linear interpolation (SLERP [37]) to compute all intermediate vectors, such that the length of the sequence is equal to the length (in frames) of the generated video. Using an interpolation rather than sampling multiple random points should enforce temporal coherency between appearances in the generated foreground. The list of latent points is then encoded through a recurrent neural network (LSTM) in order to provide a single vector (i.e., the LSTM’s final state) summarizing a representation of the whole motion. The input to the *foreground stream* is then a concatenation of the vector coming out of the LSTM and z_C , so that the generated motion can take into account the scene to which it will be applied. After a cascade of spatio-temporal convolutions (i.e., with 3D kernels that also span the time dimension), the foreground stream provides a set of frames $f(z_C, z_M)$ with foreground content and binary masks $m(z_C, z_M)$ defining motion pixel location.

The two streams are finally combined as

$$G(z_C, z_M) = m(z_C, z_M) \odot f(z_C, z_M) + (1 - m(z_C, z_M)) \odot b(z_C) \quad (1)$$

Foreground generation can be directly controlled acting on z_M . Indeed, varying z_M for a fixed value of z_C results in videos with the same background and different foreground appearance and motion. Thus, z_C can be seen as a condition for the foreground stream, in a similar way to conditional generative adversarial networks for restricting generation process to a specific class.

3.2 Discriminator Architecture

The primary goal of the discriminator network is to distinguish between generated and real videos, in order to push the generator towards more realistic outputs. At the same time, we train the discriminator to perform dense pixel-wise predictions of foreground masks and optical flow. These two additional outputs have a twofold objective: 1) they force the discriminator to learn motion-related features, rather than (for example) learn to identify the visual features of objects that are more likely to be part of the foreground (e.g., people, animals, vehicles); 2) they enable the discriminator to perform additional (and useful tasks) from unlabeled data.

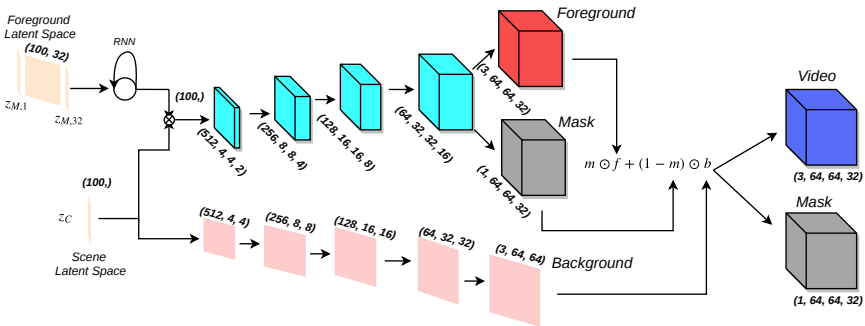


Fig. 2: **Generator architecture:** the *background stream* (bottom) is conditioned by a latent vector defining the general scene of the video, and produces a background image; the *foreground stream* (top) processes a sequence of latent vectors, obtained by spherically interpolating the start and end points, and the scene latent vector to generate frame-by-frame foreground appearance and motion masks. Information about dimensions of intermediate outputs is given in the figure by (channels, height, width, duration) tuples.

Fig. 3 shows the architecture of the discriminator. The input to the model is a video clip (either real or produced by the generator), that goes first through a series of convolutional layers, encoding the video dynamics in a more compact representation, which in turn is provided as input to two separate streams: 1) a *discrimination stream* (bottom), which applies a 3D convolution to the intermediate representation and then makes a prediction on whether the input video is real or fake; 2) a *motion stream* (top), feeding the intermediate representation to a cascade of 3D transposed convolutional layers, which fork at the final layer and return the frame-by-frame foreground segmentation maps (each as a 2D binary map) and optical flow estimations (each as a two-channel 2D map) for the input video.

The discrimination path of the model (i.e., the initial shared convolutional layers and the discrimination stream) follows a standard architecture for video discrimination [9], while the motion path, based on transposed convolutions, decodes the video representation in order to provide the two types of dense predictions [38]. Formally, we define the outputs returned by the discriminator as $D_{\text{adv}}(x)$, $D_{\text{seg}}(x)$ and $D_{\text{opt}}(x)$, which are, respectively, the probability that the provided input is real, the foreground segmentation maps and the optical flow estimated on the video; input x may be either a real video or the output of the generator.

3.3 Learning Procedure

We jointly train the generator and the discriminator in a GAN framework, with the former trying to maximize the probability that the discriminator predict fake outputs as real, and the latter trying to minimize the same probability. Additionally, when training the discriminator, we also include loss terms related to the accuracy of the estimated foreground segmentation and optical flow.

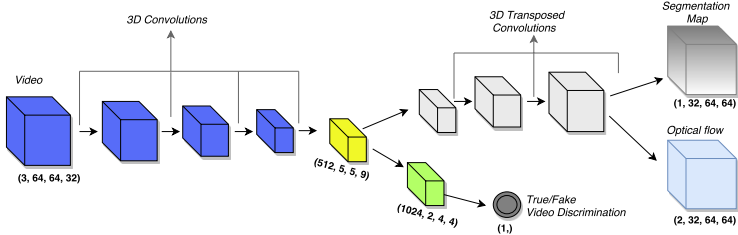


Fig. 3: **Discriminator architecture:** the *motion stream* (top) predicts foreground map and optical flow of the input video; the *discrimination stream* (bottom) outputs a single value, used for adversarial training, predicting whether the input video is real or fake.

The main problem in computing these additional losses is that, while optical flow ground truth for fake videos can be easily obtained by assuming the output of a state-of-the-art algorithm to be sufficiently accurate, there are no video segmentation approaches that provide the needed accuracy. To solve this problem, we propose what is — to the best of our knowledge — the first approach for video object segmentation trained in an unsupervised manner: since the architecture of the generator internally computes the foreground masks of the generated videos, we use those to supervise the prediction of the ones computed by the discriminator. Of course, this kind of self-referential ground-truth will not be very meaningful at first, but will become more and more akin to real ground-truth from real videos as the generator improves.

The discriminator loss is then defined as follows (for the sake of compactness, we will define $z = (z_C, z_M)$):

$$\begin{aligned}
 \mathcal{L}_D = & -\mathbb{E}_{x \sim p_{\text{real}}} [\log D_{\text{adv}}(x)] - \mathbb{E}_{x \sim p_z} [\log(1 - D_{\text{adv}}(G(z)))] \\
 & + \mathbb{E}_{z \sim p_z} \left[\frac{1}{n^2} \sum_{i,j} \text{NLL} \left(D_{\text{seg}}(G(z))_{(i,j)}, m(z)_{(i,j)} \right) \right] \\
 & + \mathbb{E}_{z \sim p_z} \left[\frac{1}{n^2} \sum_{i,j} \left(D_{\text{opt}}(G(z))_{(i,j)} - \text{OF}(G(z))_{(i,j)} \right)^2 \right] \\
 & + \mathbb{E}_{x \sim p_{\text{real}}} \left[\frac{1}{n^2} \sum_{i,j} \left(D_{\text{opt}}(x)_{(i,j)} - \text{OF}(x)_{(i,j)} \right)^2 \right]
 \end{aligned} \tag{2}$$

In the equation above, the first line encodes the adversarial loss, which pushes the discriminator to return high likelihood scores for real videos and low ones for the generated videos. The second line encodes the loss on foreground segmentation, and it computes the average pixel-wise (with coordinates (i, j) for an $n \times n$ image) negative log-likelihood of the predicted segmentation map, using the generator’s foreground mask $m(z)$ as source for correct labels (in our notation, $\text{NLL}(\hat{y}, y)$ is the negative log-likelihood of predicted label \hat{y} given correct label y). The third and fourth lines encode the loss on optical flow estimation, as the pixel-wise mean square error between the

predicted optical flow and the one calculated on the input video using the $OF(\cdot)$ function, implemented as per [39]. It should be noted that the non-adversarial term related to object segmentation is only computed on the generated videos (hence in a fully-unsupervised manner) for which foreground masks are provided by the generator in Fig. 2, since segmentation ground-truth may not be available for all real videos. Optical flow is, instead, computed on both generated and real videos, and it serves to provide supervision to the discriminator (especially to the motion stream shown in Fig. 3) in learning motion cues from real videos.

The generator loss is, more traditionally, defined as:

$$\mathcal{L}_G = -\mathbb{E}_{z \sim p_z} [\log D_{\text{adv}}(G(z))] \quad (3)$$

In this case, the generator tries to push the discriminator to increase the likelihood of its output being real.

During training, we follow the common approach for GAN training, by sampling real videos (from an existing dataset) and generated videos (from the generator) and alternately optimizing the discriminator and the generator.

4 Performance Analysis

4.1 Datasets and Metrics

Video Generation and Action Recognition. Our video generation model was trained on the “golf course” videos (over 600,000 videoclips) of the dataset proposed in [9]. We also used a standard video action recognition benchmark, UCF101 [40] (13,320 videos from 101 action categories) to evaluate how the features learned by our model are descriptive of the video content in an action recognition task.

For testing the video generation capabilities we performed qualitative and quantitative evaluation. For the former, we carried out a user study aiming at assessing how the generated videos are perceived by humans in comparison to real videos and other GAN-based generative methods, and measured the preference score in percentage. To assess video generation performance quantitatively, we evaluated separately the quality of generated background, foreground, and motion. Thus, we used the following metrics:

- **Foreground Content Distance (FCD).** This score aims at assessing the consistency between visual appearance of foreground objects in consecutive frames and is measured by computing the average L2 distance between visual features, extracted from a fully-connected layer of a pre-trained Inception network [41], of foreground objects in two consecutive frames. The input to the Inception model is the bounding box containing the foreground region, defined as the discriminator’s segmentation output.
- **Motion coherency (MC).** While the previous score describes the quality of the generated visual appearance of moving objects, this one aims at evaluating how realistic the generated motion is, and is computed as the KL-divergence between magnitude/orientation histograms of optical flows of real and generated videos.

- **Inception score (IS)** [42] is the most adopted metric in GAN literature. In our case, we compute the Inception score by sampling a random frame from each video of a pool of generated ones.

Video Object Segmentation. As a practical use case for applying adversarial models in pixel-wise dense prediction, we tested VOS-GAN on video object segmentation only. Evaluation of optical flow estimation was not performed, since our model was designed primarily for performing prediction by self-supervision (i.e., adversarial generated foreground masks), while optical flow, provided by a state-of-the-art method, was used only to guide the discriminator towards learning motion features from real videos.

For video object segmentation, we employed three datasets, namely DAVIS-16 [29], SegTrack [43] and F4K-Fish [44], containing accurate pixel-level annotations for all video frames. The three datasets show diverse features, which is useful to test the performance of video object segmentation methods in different scenarios. In particular, DAVIS-16 contains 50 full-HD videos, and includes challenging examples with occlusion, motion blur and appearance changes. SegTrack is a dataset containing 14 videos showing camera motion, slow object motion, object-background similarity, non-rigid deformations and articulated objects. F4K-Fish contains 17 videos taken in an unconstrained underwater scenario and is characterized by small objects, highly-cluttered scenes and multiple occlusions. We adopted standard metrics for video object segmentation to ease comparison between our method and state-of-the-art methods, i.e., pixel-wise intersection over union and F-measure. The results were computed on test sets when available (as in DAVIS); otherwise, we split the videos into training and test sets with proportions 70% and 30%. All available videos were divided into 32-frame shots and downsampled to fit the input size allowed by the video segmentation network, i.e., 64×64 , while output segmentation maps were rescaled (linear interpolation) to ground truth size for metrics computation.

4.2 Training Settings

Details on the generator/discriminator networks in terms of kernel sizes, padding, stride and activation functions are given, respectively, in Tab. 1 and Tab 2. In the video generation and segmentation experiments, we performed gradient-descent using ADAM, with an initial learning rate of 0.0002, $\beta_1 = 0.5$, $\beta_2 = 0.999$ and batch size of 16. We trained the video generation models for 25 epochs and the video segmentation ones for 100 epochs. For video action recognition, we used SGD with momentum and dampening of 0.9, weight decay of 0.001 and learning rate of 0.1, reduced by a factor of 10 when no improvement in validation accuracy occurred for 10 epochs. Batch size was 128 and the number of epochs was 130.

4.3 Video Generation

Qualitative evaluation. To evaluate qualitatively our video generation approach we ran a user study using Amazon Mechanical Turk (MTurk) to measure how generated videos are perceived by humans. The generated videos were compared to those synthesized by VGAN [9], TGAN [10] and to real videos. Each of the compared models was first

Bkg stream	Kernel	Stride	Padding	Activation	Output shape
z_C	—	—	—	—	100x1x1
ConvTran2D	4x4	1x1	—	LReLU($\alpha = 0.2$)	512x4x4
ConvTran2D	4x4	2x2	1x1	LReLU($\alpha = 0.2$)	256x8x8
ConvTran2D	4x4	2x2	1x1	LReLU($\alpha = 0.2$)	128x16x16
ConvTran2D	4x4	2x2	1x1	LReLU($\alpha = 0.2$)	64x32x32
ConvTran2D	4x4	2x2	1x1	Tanh	3x64x64

Fg features	Kernel Size	Stride	Padding	Activation	Output shape
$z_C, RNN(z_M)$	—	—	—	—	200x1x1
ConvTran3D	2x4x4	1x1x1	—	LReLU($\alpha = 0.2$)	512x4x4x2
ConvTran3D	3x3x3	3x3x3	1x2x2	LReLU($\alpha = 0.2$)	256x8x8x4
ConvTran3D	4x4x4	2x2x2	1x1x1	LReLU($\alpha = 0.2$)	128x16x16x8
ConvTran3D	4x4x4	2x2x2	1x1x1	LReLU($\alpha = 0.2$)	64x32x32x16

Fg raw	Kernel Size	Stride	Padding	Activation	Output shape
ConvTran3D	4x4x4	2x2x2	1x1x1	Tanh	3x64x64x32

Fg mask	Kernel Size	Stride	Padding	Activation	Output shape
ConvTran3D	4x4x4	2x2x2	1x1x1	Sigmoid	1x64x64x32

Table 1: Architecture of the generator. *Bkg stream* contains the layers included in the background stream of the model, that returns $b(z_C)$ (see Eq. 1 in the paper). *Fg features* lists the layers in the shared part of the foreground stream. The output of *Fg raw* is $f(z_C, z_M)$ and the output of *Fg mask* is $m(z_C, z_M)$. *LReLU* stands for Leaky ReLU, while the layers marked with *ConvTran* are transposed convolutions.

trained on the “golf course” videos, then two additional variants were obtained by fine-tuning the trained GAN on videos from either UCF101 or DAVIS. On MTurk, each job was created by randomly choosing two of the models under comparison and generating, for each, three 16-video batches from the three trained instances of that model; workers were then asked to choose which of the two sets of videos looked more realistic. All workers had to provide answers for all the generated batches. We took into account only the answers by workers with a lifetime Human Intelligent Task rate over than 90%. The achieved results are reported in Tab. 3 and show how our method outperformed significantly VGAN [9] and TGAN [10]. The comparison against real videos, instead, showed that our method is not yet able to reach a full level of realism, despite in 19.4% of cases our generated videos were classified as more realistic than real ones. Samples of generated videos on multiple scenes (“golf course” and UCF101) for VGAN, TGAN and our method are shown in Fig. 4. The quality of the generated videos is higher for “golf course” than UCF101 due to dataset imbalance (over 600,000 videos in the former, 13,320 in the latter).

Quantitative evaluation. Quantitative evaluation of video generation performance was carried out by measuring FCS, MC and IS scores on a set of 50,000 videos generated by the compared models trained on “golf course” [9], and on the same number of random real videos as a baseline. The results in Tab. 4 shows that VOS-GAN signifi-

Shared	Kernel Size	Stride	Padding	Activation	BatchNorm	Out shape
Input	—	—	—	—		3x64x64x32
Conv3D	4x4x4	2x2x2	1x1x1	LReLU($\alpha = 0.2$)	No	64x32x32x16
Conv3D	4x4x4	2x2x2	1x1x1	LReLU($\alpha = 0.2$)	Yes	128x16x16x8
Conv3D	4x4x4	2x2x2	1x1x1	LReLU($\alpha = 0.2$)	Yes	256x8x8x4
Conv3D	2x2x2	1x1x1	1x1x1	LReLU($\alpha = 0.2$)	Yes	512x9x9x5
Motion	Kernel Size	Stride	Padding	Activation	BatchNorm	Out shape
ConvTran3D	2x2x2	1x1x1	1x1x1	ReLU	Yes	256x8x8x4
ConvTran3D	4x4x4	2x2x2	1x1x1	ReLU	Yes	128x16x16x8
ConvTran3D	4x4x4	2x2x2	1x1x1	ReLU	Yes	64x32x32x16
ConvTran3D	4x4x4	2x2x2	1x1x1	Sigmoid	No	3x64x64x32
Discr.	Kernel Size	Stride	Padding	Activation	BatchNorm	Out shape
Conv3D	4x4x4	2x2x2	1x1x1	LReLU($\alpha = 0.2$)	Yes	1024x4x4x2
Conv3D	4x4x4	4x4x2	—	Softmax	No	2x1x1x1

Table 2: Discriminator architecture. Note that the structure of transposed convolutions used in *Motion Stream* is symmetrical to the one of convolutions in the *Shared* part. *LReLU* stands for Leaky ReLU, while the layers marked with *ConvTran* are transposed convolutions. The output of the *motion stream* has 3 channels: 1 for segmentation and 2 for optical flow.

	User preference %
VOS-GAN vs VGAN [9]	77.4 / 22.6
VOS-GAN vs TGAN [10]	62.9 / 37.1
VOS-GAN vs Real Videos	19.4 / 80.6

Table 3: User preference score (percentage) on video generation quality on different types of generated videos.

cantly outperformed VGAN and TGAN on the three metrics, achieving closer values to those yielded by real videos, indicating a higher realism in scene appearance and object motion. We also measured how the discriminator loss terms related to optical flow and segmentation affect the quality of the generated videos, by evaluating the above-mentioned metrics when either of those terms was not included in the computation. The results in Tab. 4 indicate that both terms contributed to the model’s accuracy: in particular, optical flow had the largest impact, likely because foreground regions usually correspond to clusters of oriented vectors in the optical flow, hence learning to compute it accurately is also informative from the segmentation perspective.

Finally, we tested our discriminator in a video action recognition scenario to analyze the quality of the learned motion features compared to VGAN and TGAN. In particular, we employed the discrimination networks of the three models (VOS-GAN, VGAN and TGAN) to perform video action recognition on UCF101. We tested the three models in two different training settings: a) *transfer learning*: each discriminator



Fig. 4: Frame samples on two scenes: “golf course” (top images) and UCF101 (bottom images). (First row) VGAN-generated video frames show very little object motion, while (second row) TGAN-generated video frames show motion, but the quality of foreground appearance is low. VOS-GAN (third row) generates video frames with a good compromise between object motion and appearance.

	FCD	MC	IS
VGAN [9]	10.61	0.017	1.74
TGAN [10]	3.74	0.011	2.02
VOS-GAN (w/o OF)	5.41	0.012	2.43
VOS-GAN (w/o segm.)	5.02	0.006	2.71
VOS-GAN	4.80	0.002	2.90
Real videos	4.59	0.0001	4.59

Table 4: Quantitative evaluation of video generation capabilities measured by foreground content distance (FCD), motion coherency (MC) and Inception Score (IS). “VOS-GAN (w/o OF)” is the VOS-GAN model excluding the optical flow, while “VOS-GAN (w/o segm.)” the one excluding the segmentation loss term.

was used as a feature extractor (by removing the real/fake discrimination layer) and the learned video embeddings were used to train a linear classifier; b) *fine-tuning*: we replaced the last layer of each discriminator with an apt classifier and re-trained the resulting network on UCF101 starting from the already-learned weights. To perform these tests, the starting models (before re-training according to the above two modalities) were the ones trained on the “golf course” videos and the same models fine-tuned using UCF101 as pool for real videos (indicated in Tab. 5 with UCF101 subscript). The achieved results in terms of classification accuracy are reported in Tab. 5 and show that the VOS-GAN discriminator outperformed the other two in all the considered scenarios. Lower accuracies compared to the ones reported in [9] are explained by the fact that our approach was trained only on (600,000) “golf course” raw videos, while [9] on

much more videos (over 35 million). Nevertheless, the relative performance increase of over 10% w.r.t. VGAN shows that our approach is able to achieve better representation learning capabilities in the discriminator.

Settings	Models					
	VGAN	VGAN _{UCF101}	TGAN	TGAN _{UCF101}	VOS-GAN	VOS-GAN _{UCF101}
Transfer learning	32.15	33.30	35.78	38.41	42.71	43.42
Fine-tuning	35.81	36.00	37.81	39.93	44.70	45.12

Table 5: Video Action Recognition Results on UCF101 (% classification accuracy).

4.4 Video Object Segmentation

The first part of the evaluation aimed at investigating the contribution of adversarial training for dense prediction, by assessing the quality of the foreground maps computed by our video object segmentation approach in four different training scenarios: 1) *synthetic*: we extracted the segmentation subnetwork from the architecture of our discriminator and trained it from scratch, using only the fake foreground masks coming from the generator pre-trained on “golf course”; 2) *adversarial*: we trained our GAN model on the “golf course” dataset, then used the segmentation subnetwork from the discriminator; 3) *fine-tuned synthetic*: the segmentation network trained in the *synthetic* modality was then fine-tuned on ground-truth masks of the benchmark datasets’ (DAVIS, SegTrack and F4K-Fish) training sets; 4) *fine-tuned adversarial*: analogously, we used the segmentation model from the *adversarial* training scenario fine-tuned on real segmentation masks. Tab. 6 shows the obtained performance. It can be noted that, even when the segmentation network is trained with fake data only, the resulting foreground maps on real videos are fairly good (although they are not robust to background motion). This means that the VOS-GAN generator was indeed able to generate realistic foreground maps, and the subsequent discriminator was able to extract significant features for motion areas. Fine-tuning the segmentation subnetwork on real data had the effect to focus on target objects, as shown in Fig. 5. Additionally, training the segmentation network in an adversarial framework (rather than directly on the fake maps) led to a significant performance increase, both with and without fine-tuning on real data.

We finally compared our VOS-GAN approach to state of the art video object segmentation methods, in particular with those ones not requiring any manually-annotated regions, i.e., [30,31,32,33,34,35,36,27] and achieved results are given in Tab. 7. Our GAN-based method outperformed all methods on F_1 measure, while IoU performance was lower than [27], which, however, employs CRF to improve segmentation maps, while our output maps were obtained by linearly interpolating 64×64 maps.

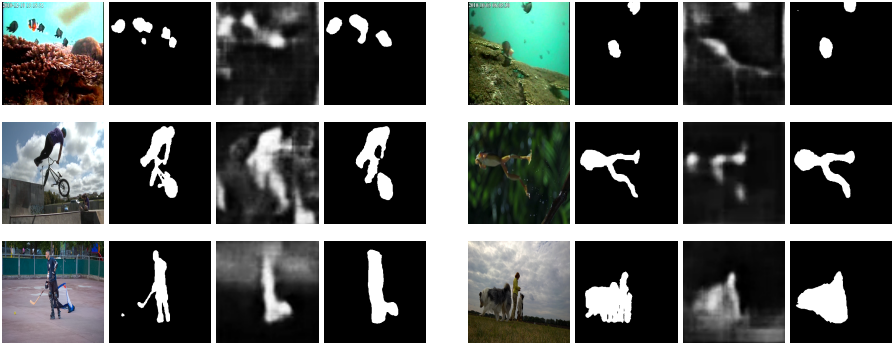


Fig. 5: **Video object segmentation results on multiple datasets.** Columns: input frame, ground truth, segmentation map obtained by the adversarial trained VOS (not thresholded, to show the detected background motion) and map computed by fine-tuning the segmentation approach on a given dataset. First row: Fish-F4k, second-row: SegTrack and third row: DAVIS.

Model	DAVIS		SegTrack		F4K-Fish	
	F_1	IoU	F_1	IoU	F_1	IoU
Synthetic VOS	43.97	28.20	47.34	31.22	33.49	20.72
Synthetic VOS fine-tuned on real data	73.13	60.41	77.93	63.85	65.98	49.51
Adversarial VOS	53.82	37.19	60.45	43.36	42.23	27.00
Adversarial VOS fine-tuned on real data	80.31	67.74	81.53	69.00	70.13	54.36

Table 6: Video segmentation results (percentage). The first two rows are the ones achieved without adversarial training, respectively, before and after fine-tuning on real data. The last two rows, instead, are the results yielded by adversarial training, respectively, before and after fine-tuning.

	[30]	[31]	[32]	[33]	[34]	[35]	[36]	[27]	VOS-GAN
F_1	26.4	57.9	43.7	53.4	61.3	51.9	57.8	78.3	80.3
IoU	38.6	65.2	44.3	67.1	63.6	56.0	58.1	82.9	67.7

Table 7: Comparison to state-of-the-art methods on DAVIS with F-Measure (F_1) and intersection over union (IoU), in percentage. All values, except VOS-GAN, taken from [27] and [29].

5 Conclusion

We propose a novel GAN-based video generation approach — VOS-GAN — that employs two input latent spaces: one for modeling the background, and one to model foreground motion and appearance. In addition, motion generation is improved by controlling the discrimination process with pixelwise dense prediction of moving objects. Beside the generation process, the proposed framework allows us to perform video object segmentation and optical flow estimation. Extensive experimental evaluation showed

that our VOS-GAN outperforms significantly existing GAN-based methods, VGAN [9] and TGAN [10], on the video generation process, by creating videos with more realistic motion (measured both qualitatively and quantitatively). Moreover, performance analysis on video object segmentation tasks revealed that our approach is effectively able to learn video dynamics for dense prediction in an unsupervised way.

References

1. Goodfellow, I., Pouget-Abadie, J., Mirza, M., Xu, B., Warde-Farley, D., Ozair, S., Courville, A., Bengio, Y.: Generative adversarial nets. In Ghahramani, Z., Welling, M., Cortes, C., Lawrence, N.D., Weinberger, K.Q., eds.: *Advances in Neural Information Processing Systems 27*. Curran Associates, Inc. (2014) 2672–2680
2. Denton, E.L., Chintala, S., Szlam, A., Fergus, R.: Deep generative image models using a laplacian pyramid of adversarial networks. In Cortes, C., Lawrence, N.D., Lee, D.D., Sugiyama, M., Garnett, R., eds.: *Advances in Neural Information Processing Systems 28*. Curran Associates, Inc. (2015) 1486–1494
3. Radford, A., Metz, L., Chintala, S.: Unsupervised representation learning with deep convolutional generative adversarial networks. *ICLR* (2016)
4. Zhang, H., Xu, T., Li, H., Zhang, S., Wang, X., Huang, X., Metaxas, D.N.: Stackgan: Text to photo-realistic image synthesis with stacked generative adversarial networks. In: *The IEEE International Conference on Computer Vision (ICCV)*. (Oct 2017)
5. Arjovsky, M., Chintala, S., Bottou, L.: Wasserstein generative adversarial networks. In Precup, D., Teh, Y.W., eds.: *Proceedings of the 34th International Conference on Machine Learning*. Volume 70 of *Proceedings of Machine Learning Research*, International Convention Centre, Sydney, Australia, PMLR (06–11 Aug 2017) 214–223
6. Mao, X., Li, Q., Xie, H., Lau, R.Y., Wang, Z., Paul Smolley, S.: Least squares generative adversarial networks. In: *The IEEE International Conference on Computer Vision (ICCV)*. (Oct 2017)
7. Roth, K., Lucchi, A., Nowozin, S., Hofmann, T.: Stabilizing training of generative adversarial networks through regularization. In Guyon, I., Luxburg, U.V., Bengio, S., Wallach, H., Fergus, R., Vishwanathan, S., Garnett, R., eds.: *Advances in Neural Information Processing Systems 30*. Curran Associates, Inc. (2017) 2018–2028
8. Huang, X., Li, Y., Poursaeed, O., Hopcroft, J., Belongie, S.: Stacked generative adversarial networks. In: *The IEEE Conference on Computer Vision and Pattern Recognition (CVPR)*. (July 2017)
9. Vondrick, C., Pirsivash, H., Torralba, A.: Generating videos with scene dynamics. In Lee, D.D., Sugiyama, M., Luxburg, U.V., Guyon, I., Garnett, R., eds.: *Advances in Neural Information Processing Systems 29*. Curran Associates, Inc. (2016) 613–621
10. Saito, M., Matsumoto, E., Saito, S.: Temporal generative adversarial nets with singular value clipping. In: *The IEEE International Conference on Computer Vision (ICCV)*. (Oct 2017)
11. Walker, J., Doersch, C., Gupta, A., Hebert, M.: An uncertain future: Forecasting from static images using variational autoencoders. In Leibe, B., Matas, J., Sebe, N., Welling, M., eds.: *Computer Vision – ECCV 2016*, Cham, Springer International Publishing (2016) 835–851
12. Larsen, A.B.L., Sønderby, S.K., Larochelle, H., Winther, O.: Autoencoding beyond pixels using a learned similarity metric. In: *Proceedings of the 33rd International Conference on International Conference on Machine Learning - Volume 48. ICML’16, JMLR.org* (2016) 1558–1566

13. Gregor, K., Danihelka, I., Graves, A., Rezende, D., Wierstra, D.: Draw: A recurrent neural network for image generation. In Bach, F., Blei, D., eds.: Proceedings of the 32nd International Conference on Machine Learning. Volume 37 of Proceedings of Machine Learning Research., Lille, France, PMLR (07–09 Jul 2015) 1462–1471
14. Srivastava, N., Mansimov, E., Salakhutdinov, R.: Unsupervised learning of video representations using lstms. In: Proceedings of the 32Nd International Conference on International Conference on Machine Learning - Volume 37. ICML'15, JMLR.org (2015) 843–852
15. Oh, J., Guo, X., Lee, H., Lewis, R., Singh, S.: Action-conditional video prediction using deep networks in atari games. In: Proceedings of the 28th International Conference on Neural Information Processing Systems - Volume 2. NIPS'15, Cambridge, MA, USA, MIT Press (2015) 2863–2871
16. Finn, C., Goodfellow, I., Levine, S.: Unsupervised learning for physical interaction through video prediction. In Lee, D.D., Sugiyama, M., Luxburg, U.V., Guyon, I., Garnett, R., eds.: Advances in Neural Information Processing Systems 29. Curran Associates, Inc. (2016) 64–72
17. Xue, T., Wu, J., Bouman, K., Freeman, B.: Visual dynamics: Probabilistic future frame synthesis via cross convolutional networks. In Lee, D.D., Sugiyama, M., Luxburg, U.V., Guyon, I., Garnett, R., eds.: Advances in Neural Information Processing Systems 29. Curran Associates, Inc. (2016) 91–99
18. Villegas, R., Yang, J., Hong, S., Lin, X., Lee, H.: Decomposing motion and content for natural video sequence prediction. ICLR (2017)
19. Vondrick, C., Torralba, A.: Generating the future with adversarial transformers. In: The IEEE Conference on Computer Vision and Pattern Recognition (CVPR). (July 2017)
20. Bousmalis, K., Silberman, N., Dohan, D., Erhan, D., Krishnan, D.: Unsupervised pixel-level domain adaptation with generative adversarial networks. In: The IEEE Conference on Computer Vision and Pattern Recognition (CVPR). (July 2017)
21. Tzeng, E., Hoffman, J., Saenko, K., Darrell, T.: Adversarial discriminative domain adaptation. In: The IEEE Conference on Computer Vision and Pattern Recognition (CVPR). (July 2017)
22. Zhu, J.Y., Park, T., Isola, P., Efros, A.A.: Unpaired image-to-image translation using cycle-consistent adversarial networks. In: The IEEE International Conference on Computer Vision (ICCV). (Oct 2017)
23. Yi, Z., Zhang, H., Tan, P., Gong, M.: Dualgan: Unsupervised dual learning for image-to-image translation. In: The IEEE International Conference on Computer Vision (ICCV). (Oct 2017)
24. Souly, N., Spampinato, C., Shah, M.: Semi supervised semantic segmentation using generative adversarial network. In: The IEEE International Conference on Computer Vision (ICCV). (Oct 2017)
25. Mahasseni, B., Lam, M., Todorovic, S.: Unsupervised video summarization with adversarial lstm networks. In: The IEEE Conference on Computer Vision and Pattern Recognition (CVPR). (July 2017)
26. Lai, W.S., Huang, J.B., Yang, M.H.: Semi-supervised learning for optical flow with generative adversarial networks. In Guyon, I., Luxburg, U.V., Bengio, S., Wallach, H., Fergus, R., Vishwanathan, S., Garnett, R., eds.: Advances in Neural Information Processing Systems 30. Curran Associates, Inc. (2017) 354–364
27. Tokmakov, P., Alahari, K., Schmid, C.: Learning motion patterns in videos. In: Proceedings of IEEE Conference on Computer Vision and Pattern Recognition. (2017)
28. Krähenbühl, P., Koltun, V.: Efficient inference in fully connected crfs with gaussian edge potentials. In Shawe-Taylor, J., Zemel, R.S., Bartlett, P.L., Pereira, F., Weinberger, K.Q., eds.: Advances in Neural Information Processing Systems 24. Curran Associates, Inc. (2011) 109–117

29. Perazzi, F., Pont-Tuset, J., McWilliams, B., Gool, L.V., Gross, M., Sorkine-Hornung, A.: A benchmark dataset and evaluation methodology for video object segmentation. In: 2016 IEEE Conference on Computer Vision and Pattern Recognition (CVPR). (June 2016) 724–732
30. Wang, W., Shen, J., Porikli, F.: Saliency-aware geodesic video object segmentation. In: 2015 IEEE Conference on Computer Vision and Pattern Recognition (CVPR). (June 2015) 3395–3402
31. Papazoglou, A., Ferrari, V.: Fast object segmentation in unconstrained video. In: 2013 IEEE International Conference on Computer Vision. (Dec 2013) 1777–1784
32. Bideau, P., Learned-Miller, E.G.: It’s moving! A probabilistic model for causal motion segmentation in moving camera videos. In: Computer Vision - ECCV 2016 - 14th European Conference, Amsterdam, The Netherlands, October 11-14, 2016, Proceedings, Part VIII. (2016) 433–449
33. Lee, Y.J., Kim, J., Grauman, K.: Key-segments for video object segmentation. In: 2011 International Conference on Computer Vision. (Nov 2011) 1995–2002
34. Brox, T., Malik, J.: Object segmentation by long term analysis of point trajectories. In: Proceedings of the 11th European Conference on Computer Vision: Part V. ECCV’10, Berlin, Heidelberg, Springer-Verlag (2010) 282–295
35. Fragkiadaki, K., Zhang, G., Shi, J.: Video segmentation by tracing discontinuities in a trajectory embedding. In: 2012 IEEE Conference on Computer Vision and Pattern Recognition. (June 2012) 1846–1853
36. Taylor, B., Karasev, V., Soatto, S.: Causal video object segmentation from persistence of occlusions. In: 2015 IEEE Conference on Computer Vision and Pattern Recognition (CVPR). (June 2015) 4268–4276
37. Shoemake, K.: Animating rotation with quaternion curves. SIGGRAPH Comput. Graph. **19**(3) (July 1985) 245–254
38. Badrinarayanan, V., Kendall, A., Cipolla, R.: Segnet: A deep convolutional encoder-decoder architecture for image segmentation. IEEE Transactions on Pattern Analysis and Machine Intelligence (2017)
39. Farnebäck, G.: Two-frame motion estimation based on polynomial expansion. In: Proceedings of the 13th Scandinavian Conference on Image Analysis. SCIA’03, Berlin, Heidelberg, Springer-Verlag (2003) 363–370
40. Soomro, K., Zamir, A.R., Shah, M.: UCF101: A dataset of 101 human actions classes from videos in the wild. CoRR **abs/1212.0402** (2012)
41. Szegedy, C., Liu, W., Jia, Y., Sermanet, P., Reed, S., Anguelov, D., Erhan, D., Vanhoucke, V., Rabinovich, A.: Going deeper with convolutions. In: Computer Vision and Pattern Recognition (CVPR). (2015)
42. Salimans, T., Goodfellow, I., Zaremba, W., Cheung, V., Radford, A., Chen, X., Chen, X.: Improved techniques for training gans. In Lee, D.D., Sugiyama, M., Luxburg, U.V., Guyon, I., Garnett, R., eds.: Advances in Neural Information Processing Systems 29. Curran Associates, Inc. (2016) 2234–2242
43. Tsai, D., Flag, M., Nakazawa, A., Rehg, J.M.: Motion coherent tracking using multi-label mrf optimization. International Journal of Computer Vision **100**(2) (Nov 2012) 190–202
44. Kavasidis, I., Palazzo, S., Salvo, R.D., Giordano, D., Spampinato, C.: An innovative web-based collaborative platform for video annotation. Multimedia Tools Appl. **70**(1) (May 2014) 413–432